Article

How Land Use Transitions Contribute to the Soil Organic Carbon Accumulation from 1990 to 2020

Zihui Zhang , Lang Xia , Zifei Zhao , Fen Zhao , Guanyu Hou , Shixin Wu , Xiao Sun , Shangrong Wu , Peng Yang , Yan Zha *

Posted Date: 29 February 2024

doi: 10.20944/preprints202402.1659.v1

Keywords: Soil organic carbon density; Soil organic carbon stocks; Land use change; Sparrow search algorithm; Alpine mountains region

 doi:10.20944/preprints202402.1659.v1

Article

How Land Use Transitions Contribute to the Soil Organic Carbon Accumulation from 1990 to 2020

Zihui Zhang [1,2], Lang Xia [1,2], Zifei Zhao [3], Fen Zhao [1,2,*], Guanyu Hou [4], Shixin Wu [4], Xiao Sun [1,2], ShangRong Wu [1,2], Peng Yang [1,2] and Yan Zha [2,*]

[1] State Key Laboratory of Efficient Utilization of Arid and Semi-arid Arable Land in Northern China, the Institute of Agricultural Resources and Regional Planning, Chinese Academy of Agricultural Sciences, Beijing 100081, China
[2] Institute of Agricultural Resources and Regional Planning, Chinese Academy of Agricultural Sciences/Key Laboratory of Agricultural Remote Sensing, Ministry of Agriculture and Rural Affairs, Beijing 100081, China
[3] Key Laboratory of Space Utilization, Chinese Academy of Sciences, Beijing 100091, China
[4] State Key Laboratory of Desert and Oasis Ecology, Xinjiang Institute of Ecology and Geography, Chinese Academy of Sciences, Urumqi 830011, Xinjiang, China
* Correspondence: zhayan@caas.cn

Abstract: SOC stock (SOCS) changes caused by land use changes are still unclear, and understanding this response is essential for many environmental policies and land management practices. In this study, we investigated the temporal-spatial and vertical distribution characteristics of SOCS on the Western Sichuan Plateau (WSP) using the sparrow search algorithm-random forest regression (SSA-RFR) models with excellent model applicability and accuracy. The temporal-spatial variations in the SOCS were modeled using 1080 soil samples and a set of nine environmental covariates. We analyzed the effect of land use changes on the SOCS on the WSP. The total SOCS increased by 18.03 Tg C from 1990 to 2020. The results of this study confirmed that the SOCS in the study area has increased significantly since 2010, with an increase of 27.88 Tg C compared to the total SOCS in 2010. We found that the spatial distribution of the SOCS increased from southeast to northwest, and the vertical distribution of the SOCS in the study area decreased with increasing soil depth. Forest and grassland are the main sources of SOCS, the total SOCS in the forest and grassland accounted for 37.53 and 59.39% of the total SOC pool in 2020, respectively. Expansion of the wetlands, forest, and grassland areas could increase SOCS in the study area.

Keywords: Soil organic carbon density; Soil organic carbon stocks; Land use change; Sparrow search algorithm; Alpine mountains region

1. Introduction

Soil organic carbon (SOC) is a significant indicator to measure soil fertility and evaluate crop growth and development [1,2]. It is related to climate change [3], vegetation types [4], land use change (LUC) [5,6], and human activities [7]. As land resource management transitions from quantity-focused to quality-focused management [8], it is crucial to study the effect of this transition on SOC stock (SOCS). In addition, the response of SOCS to land use change across different soil layers and regions, and it is essential to examine the impact of land use change on SOCS in both horizontal and vertical directions [9]. SOC, pH, and soil bulk density (SBD) are important indicators for estimating SOCS [10]. Accurate estimation of these parameters is crucial for assessing regional changes in SOCS and understanding carbon cycles in ecosystems. Studying the temporal-spatial characteristic of LUC plays an important part in the exploration of the change of SOCS. However, only a few studies have focused on the effects of LUC on the SOCS using a long time-series [5,6,11–13]. Therefore, it is significant to investigate the effects of LUC on the SOCS.

At present, random forest regression (RFR) has been commonly used to estimate the SOC and SBD based on multi-source remote sensing data, and these models have strong applicability [14–16].

 doi:10.20944/preprints202402.1659.v1

To further improve the accuracy of RFR model, the sparrow search algorithm (SSA) can be employed, which is known for its easy implementation, versatility, and fast convergence speed. [17,18]. In addition, it is vital to identify the major environmental variables affecting the SOC content, these variables groups were utilized as input dataset for SOC prediction models. However, the optimal combination of these variables for improving the modeling accuracy has different performance in different regions, it is urgent for us to find the optimal combination for the specific region.

The Qinghai–Tibet Plateau (QTP) is an important region for studying carbon sinks and global energy, carbon, and moisture cycles [10,12]. However, the effect of LUC on the increase in SOCS in the QTP is still unclear. It is essential to qualitatively and quantitatively investigate the SOC effects and potential risk assessment. Some studies have reported that LUC can directly affect the SOCS [19,20], while others have indicated that LUC are affected by climate change, indirectly affecting the SOCS [3,12,21,22]. Many scholars have regarded the QTP as their study area to investigate the changes in the SOCS with coarse spatial resolution (e.g., 90 m, 250 m, 500 m, 1000 m) and short time series, their results have some limitations in showing the fine spatial and temporal characteristics in QTP [12,23,24]. To address these limitations, this study focused on the Western Sichuan Plateau (WSP), which is located in the southeastern part of the QTP. The WSP is known for its natural ecosystems, including forests, grassland, and wetlands, which have a prominent carbon reduction effect [25]. The WSP is a major pastoral areas in China, with grasslands plays a critical role [26]. The WSP is a sensitive area, in which the vegetation types and soil conditions are closely related to climate conditions [27]. Understanding the effects of LUC on the SOCS is important for developing practices that promote agricultural sustainability. However, only a few studies have been related to the SOCS on the WSP [28–30], and it is important to study the impact of LUC on the SOCS in the WSP.

In this study, we analyzed the impact of LUC on the temporal-spatial variability of the SOCS in the WSP based on long time-series field survey data and SSA-RFR. We measured the SOC content, pH, and SBD of the topsoil (0–5, 5–10, 10–20, and 20–30 cm) using data for 54 sampling sites to estimate the spatial and vertical distribution of the SOC and SBD. We analyzed the temporal-spatial and vertical trends of the SOCS under LUC from 1990 to 2020. The optimal combination of environmental covariates with a highest model accuracy was determined by the different characteristics of SOC and SBD in different soil layers. Then, SSA-RFR was used to build SOC and SBD estimation models for the WSP, the optimal models were adopted to upscale the field survey samples to the whole of study region. The spatial distribution results of the SOC density (SOCD) were mapped with a high-resolution (30 m). Understanding the factors driving SOC dynamics is crucial for developing effective land management strategies to enhance carbon sequestration and mitigate land degradation.

2. Materials and Methods

2.1. Study Areas

The WSP is located in the southeastern part of the QTP (27°28′15.6″–34°18′46.8″N, 97°20′56.4″–104°42′50.4″E; Figure 1), with an average elevation of 4177 m, and the total area of about 2.98 × 105 km^2. The average annual temperature was 7.5°C and the average annual precipitation was 87.61 mm in 2020 (Figure 1b). The main soil types are dark felty soils, felty soils, and brown earths (Figure 1d). *Carex myosuroides* Vill. and a variety of grass vegetation mostly grow in the dark felty soil, and it is an important area for livestock products. The vegetation in the alpine meadows is mainly *Kobresia humilis* and *Carex alatauensis* S. R. Zhang, and the accompanying species include *Carex tristachya* Thunb. and *Polygonum macrophyllum* D. Don [31].

 doi:10.20944/preprints202402.1659.v1

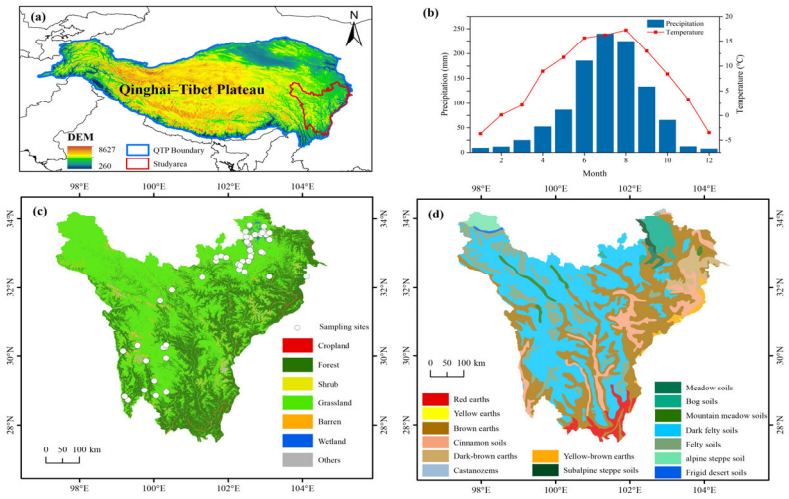

Figure 1. (a) Location of the study area. (b) Monthly mean precipitation and temperature data for the study area in 2020. (c) Land use data in 2020 and spatial distribution of the SOC sampling sites. (d) Map of the soil types in the study area.

2.2. Field Data Measurements and Processes

We collected a total of 1080 soil samples from August 2018 to August 2020, the sampling sites were evenly distributed and representative (Figure 1c). In each sampling area, five samples were collected at equidistant locations to obtain average values. Additionally, two 100 m sample lines were established in each sampling area (Figure 2a). For each sample, we collected undisturbed soil samples at fixed intervals of 0–5, 5–10, 10–20, and 20–30 cm in the topsoil layer using steel bulk density rings (Figure 2b). These samples were oven dried at 105°C until a constant mass was achieved to determine the SBD (g cm^{-3}). The SOC content of the samples was separately determined using potassium dichromate oxidation-spectrophotometry. To estimate SOCS, we calculated the SOCD in a certain soil layer thickness per unit area (1 m^2). The SOCS in the 0–30 cm layer was calculated using equation (1) [32–34].

$$SOCS = A \times \sum_{i=1}^{n} SOCD\,, SOCD = SOC_i \times H_i \times SBD_i \times \frac{1-G_i}{100}, \quad (1)$$

where A is the area of the study area (m^2); SOCD is the density of SOC (t hm^{-2}); H is the soil thickness (cm); SBD is the bulk density of the soil layer (g cm^{-3}); G is the gravel content of the soil sample (%); and n is the number of soil layers (n = 4).

Figure 2. Schematic diagram of the sampling area. (a) Distribution of the samples in each sampling area. (b) Schematic diagram of the soil profile.

To ensure the accuracy and reliability of the spatiotemporal analysis of the SOCS, many relevant measured data were obtained from several articles to validate and correct the results of this study [15,23,35–38].Moreover, publicly available soil data (including the SBD and SOC data for the 0–30 cm soil layer(s) in the 2010s) were acquired from the above studies, and some of the soil data (including SBD data for the 0–30 cm soil layer) were obtained from the Harmonized World Soil Database

 doi:10.20944/preprints202402.1659.v1

(HWSD). This database provided us with additional SBD data for the 0-30 cm soil layer. By incorporating these diverse sources of data, we aimed to enhance the robustness and comprehensiveness of our analysis.

2.3. Satellite Data and Pre-Processing

Landsat is a widely used optical remote sensing satellite that provides multispectral data and has the longest continuous airborne observations in the world [39]. In this study, we collected a series of Landsat remote sensing data during the vegetation growth periods in the study area. This included Landsat-5 Thematic Mapper (TM) sensor images for 1990 and 2000, Landsat-7 Enhanced Thematic Mapper Plus (ETM+) sensor images for 2010, and Landsat-8 Operational Land Imager (OLI) images for 2020. A total of 224 Landsat scenes were downloaded from the United States Geological Survey Earth Explorer (USGS EarthExplorer, https://earthexplorer.usgs.gov/)with the image acquisition time was close to the field measurement time and the cloud cover of less than 10%. The images were pre-processed using the ENVI software. The vegetation indices were calculated by band math (Table 1). Moreover, a digital elevation model (DEM) was obtained from shuttle radar topography mission (SRTM) images (https://lpdaac.usgs.gov/products/srtmgl1v003/, version 003, 30 m), which was used to calculate the slope, aspect, terrain ruggedness index (TRI) and topographic wetness index (TWI). Both the above vegetation indices and terrain indicators were used to construct the dataset for the RFR model. The land use change data were obtained from the National Land Use Dataset (NLUD). The meteorological and LUC data were used to analyze the spatial and temporal characteristics of the SOC and SBD.

Table 1. Selected vegetation indices and calculation formulae.

Vegetation indices	Equations	References
NDVI	$\frac{R_{nir} - R_{red}}{R_{nir} + R_{red}}$	[16]
EVI	$\frac{2.5 * (R_{nir} - R_{red})}{R_{nir} + 6R_{red} - 7R_{blue} + 1}$	[40]
CI_g	$\frac{R_{nir}}{R_{green}} - 1$	[41]
SAVI	$\frac{1.5 * (R_{nir} - R_{red})}{R_{nir} + R_{red} + 0.5}$	[42]

* Note: NDVI: normalized difference vegetation index; EVI: enhanced vegetation index; CIg: chlorophyll index-green; SAVI: soil-adjusted vegetation index.

2.4. Random Forest Regression Model and Accuracy Evaluation

Random forest regression (RFR) algorithm is a machine learning algorithm that is known for its fast computation, high accuracy, and a strong anti-overfitting capability [43]. It has been widely utilized to estimate the ecological indicators [44]. In the RFR model, the predicted value of an observation is calculated by averaging over all of the trees. This helps to avoid the limitations of a single decision tree and improves the performance by reducing the model variance [44,45]. In this study, 70% of the soil samples were utilized as the training set, and 30% of soil samples were utilized as the testing set. To ensure the optimal and stable model, five-fold cross validation was employed to evaluate the performance of the RFR models. The performance of the RFR models of the SBD and SOC predictions were evaluated using the coefficient of determination (R^2, equation (2)), mean absolute error (MAE, equation (3)), root mean square error (RMSE, equation (4)), and BIAS (equation (5)) [40,45].

$$R^2 = 1 - \frac{\sum_{i=1}^{n}(y_i - f_i)^2}{\sum_{i=1}^{n}(y_i - \overline{y})^2}, \quad (2)$$

$$MAE = \frac{\sum_{i=1}^{n}|\hat{y}_i - y_i|}{n}, \quad (3)$$

 doi:10.20944/preprints202402.1659.v1

$$RMSE = \sqrt{\frac{\sum_{i=1}^{n}(y_i - f_i)^2}{n}}, \quad (4)$$

$$BIAS = \bar{y} - \bar{f}, \quad (5)$$

where y_i and f_i represents the field measured and estimated SOC or SBD values in the i_{th} sample, respectively, $\bar{y}$ and $\bar{f}$ are the measured and estimated SOC or SBD averaged over all of the soil samples, and n is the number of soil samples.

2.5. Sparrow Search Algorithm

The sparrow search algorithm is an emerging optimization algorithm introduced in 2020. It draws inspiration from the foraging behavior of sparrows and applies cooperative and competitive strategies to find the most optimal solutions within the solution space [46]. The SSA incorporates randomness and local search mechanisms to enhance its ability to explore the solution space and improve the convergence of the algorithm [47]. It can be used to optimize the parameters in the RFR model, such as the number of decision trees, maximum depth, and feature selection. By optimizing these parameters, the SSA aims to achieve a model with a better performance. However, it is worth noting that the SSA requires a large number of iterations and model evaluations, which can result in a high computational complexity. This means that running the SSA may take a long time and require significant computational resources.

3. Results

3.1. Statistical Analysis of SBD and SOC

The vertical distribution of the SOC decreased with increasing soil depth, with an average SOC value of 66.12 g kg^{-1} in the 0–30 cm layer (Figure 3). The largest decrease in the SOC content occurred between 5–10 cm and 0–5 cm and in adjacent soil layers, with a maximum difference of 117.26 g kg^{-1}. The average SBD value for the 0–30 cm interval in the study area was 0.83 g cm^{-3}. SBD and SOC content in 0–5 cm soil layer was strongly influenced by land management patterns.

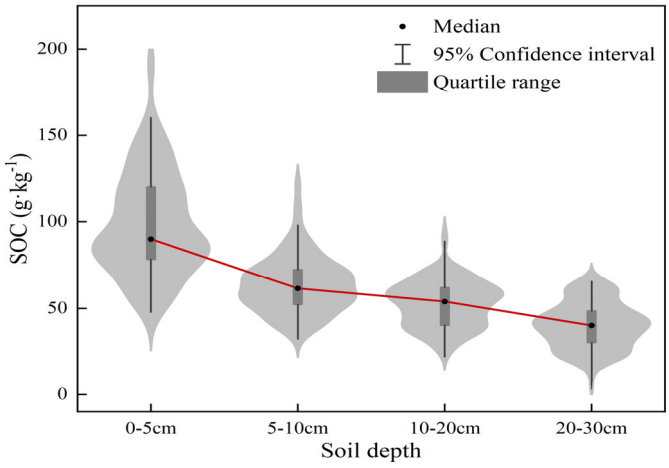

Figure 3. SOC content in different soil depths.

Both the pH and SBD exhibited significant negative correlations with the SOC (Figure 4). Soil is rich in microorganisms which are suitable to grow in neutral soil environment. The study area is an acidic soil, in which the decomposition process of organic carbon is inhibited and can increase the stability of SOC. SOC has the ability to combined with soil particles, enhancing soil stability and reducing SBD. Additionally, higher SOC in the soil result in increased microbial activity and soil biodiversity, which facilitate the breakdown and decomposition of soil organic matter in the soil. This

 doi:10.20944/preprints202402.1659.v1

process contribute to the formation of soil aggregates and improves soil structure and reduces soil compaction.

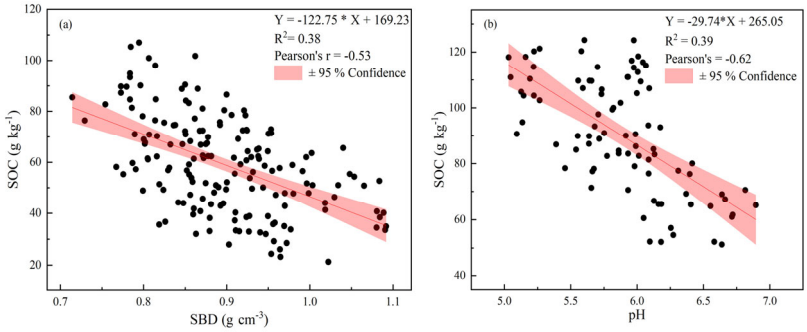

Figure 4. The linear relationships between the SBD and the SOC, pH, and SOC.

The average SOCD value in the 0–30 cm was 1.98 t hm^{-2}. The SOCD decreased with increasing soil depth. And there were noticeable differences in the SOCD among the different land use types (Figure 5). SOCD can directly influence SOCS. Vegetation types and land use types strongly influence SOCD and SOCS. For example, ploughing and agricultural activities lead to a decrease in SOC, whereas natural ecosystems such as forests and grasslands can contribute to the accumulation of SOC.

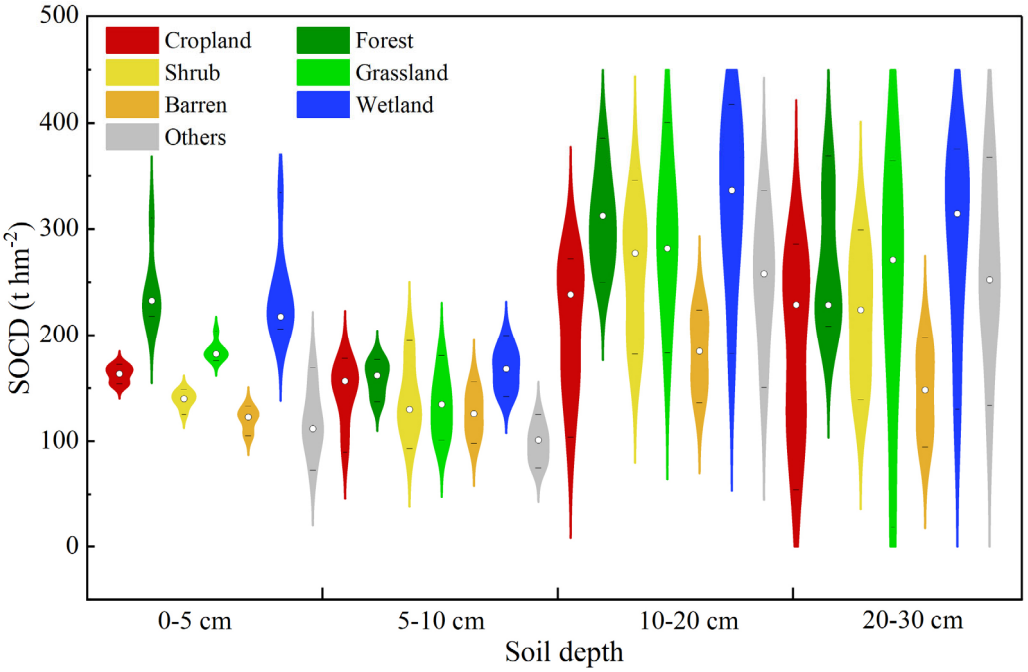

Figure 5. SOCD of different land use types in the 0–30 cm interval. The white dots indicate the median and the upper and lower lines denote the maximum and minimum values of the SOCD.

3.2. Applicability of SSA-RFR Model

SSA-RFR models were used to construct the SBD and SOC estimation models for the study area. The indicator significance results for each model also exhibited significant differences (Figure 6). According to the indicator significance results, the DEM, we chose the mainly indicators to estimate SBD and SOC in each different soil layers. This is because different spectral bands reflect different vegetation properties and hence soil properties. Topographic indices can reflect soil properties and compensate for the limitations of remotely sensed data in obtaining surface data. Therefore, the combination groups of these vegetation and topographic indicators are a good description of the soil properties.

 doi:10.20944/preprints202402.1659.v1

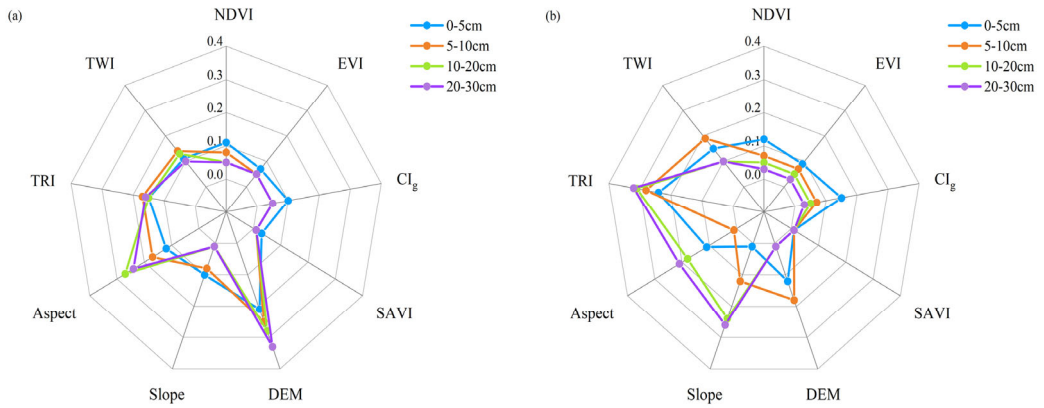

Figure 6. Importance of indicators in the SSA-RFR models for estimating the (a) and (b) SOC in the different soil layers.

The optimal SBD and SOC in the different soil depth estimation models were selected to achieve the point-to-region expansion based on the cross validation. The precision evaluation indicators of SSA-RFR models are listed in Table 2. The simulated SBD and SOC exhibited strong correlations with the measured SBD and SOC across each model (Figure 7). The estimation accuracy of the SBD prediction model was significantly better than that of the SOC prediction model. Moreover, all of the SSA-RFR models have strong stability and applicability in SBD and SOC estimation. We validated the results of the SBD and SOC in different years using datasets obtained from the relevant studies and the HWSD (Figure 7). Our results have an excellent consistency with the validation data.

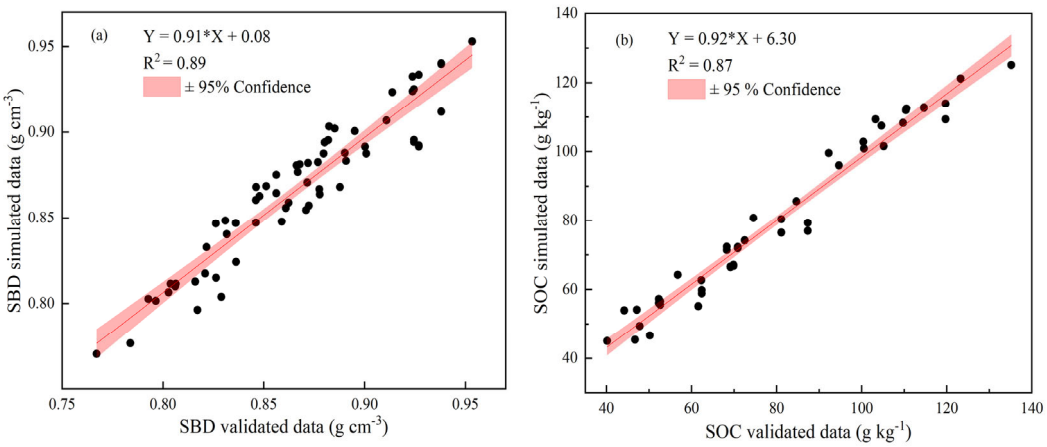

Figure 7. Validation of simulated data using measured data. (a) Validation of SBD. (b) Validation of SOC.

Table 2. SSA-RFR model evaluation indicators for SBD and SOC prediction in different soil layers.

SSA-RFR model		R^2	MAE	RMSE	BIAS	Accuracy
SBD	0–5 cm	0.79	0.09	0.13	0.14	94.38%
	5–10 cm	0.76	0.08	0.09	0.02	92.13%
	10–20 cm	0.74	0.06	0.08	0.06	93.34%
	20–30 cm	0.78	0.06	0.08	0.05	93.79%
SOC	0–5 cm	0.62	18.09	21.63	0.06	82.43%
	5–10 cm	0.67	10.31	12.92	0.17	82.69%
	10–20 cm	0.65	9.44	10.91	0.23	80.25%
	20–30 cm	0.62	10.38	12.68	0.36	82.28%

* Note: SBD: soil bulk density; SOC: soil organic carbon.

 doi:10.20944/preprints202402.1659.v1

3.3. Spatial Distribution of SOCD in 2020

Using the nine spatial explanatory variables and the optimized SSA-RFR models for the different soil layers (within 0–30 cm), we generated a map of the SOCD in 2020 (Figure 8). The SOCD was higher in the northern and western parts of the study area. In addition, the wetlands had the highest SOCD in the WSP, and the magnitude of the decrease in the SOCD with increasing soil depth were different.

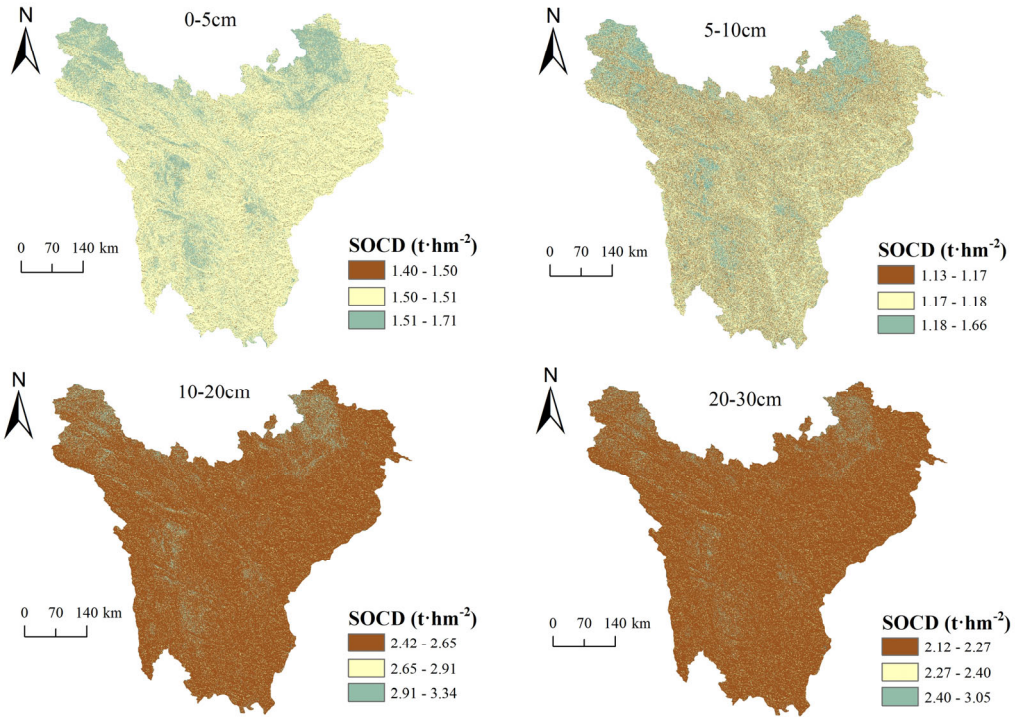

Figure 8. Spatial distribution of the SOCD at different soil depths in the WSP obtained using the SSA-RFR models.

Combined with the land use data for the WSP, we calculated the SOCS of the different land use types at different soil depths (Table 3). The grassland had the highest SOCS in the WSP. The total SOCS in the study area in 2020 was 232.94 Tg. The total SOCS of the seven land use types in topsoil were different. The SOCS of the forest, shrub, and grassland remained stable and can be fixed in the soil for long periods.

Table 3. Statistics of the SOCS in topsoil for the different land use types.

Land use type	Area (km²)	SOCS (Tg C)			
		0–5 cm	5–10 cm	10–20 cm	20–30 cm
Cropland	1562	0.24	0.19	0.41	0.34
Forest	105251	18.11	15.60	29.31	25.39
Shrub	3014	0.45	0.36	0.78	0.61
Grassland	179529	27.20	21.70	49.21	40.21
Barren land	5436	0.66	0.55	1.09	1.04
Wetland	528	0.10	0.08	0.15	0.14
Others	2330	0.0039	0.0029	0.0062	0.0056
All	297650	46.7639	37.4829	80.9562	67.7356

 doi:10.20944/preprints202402.1659.v1

3.4. Characteristics of Temporal-Spatial Distribution of SOCD

The average SOCD values were 7.21, 7.06, 6.88, and 7.82 t hm^{-2} in 1990, 2000, 2010, and 2020, respectively (Figure 9). The total SOCD increased by 0.61 t hm^{-2} from 1990 to 2020. The greatest increasing trend of SOCD occurred in the northern and western regions of the study area, which were mostly grassland and forest areas. The total SOCD decreased from 1990 to 2010 and increased from 2010 to 2020.

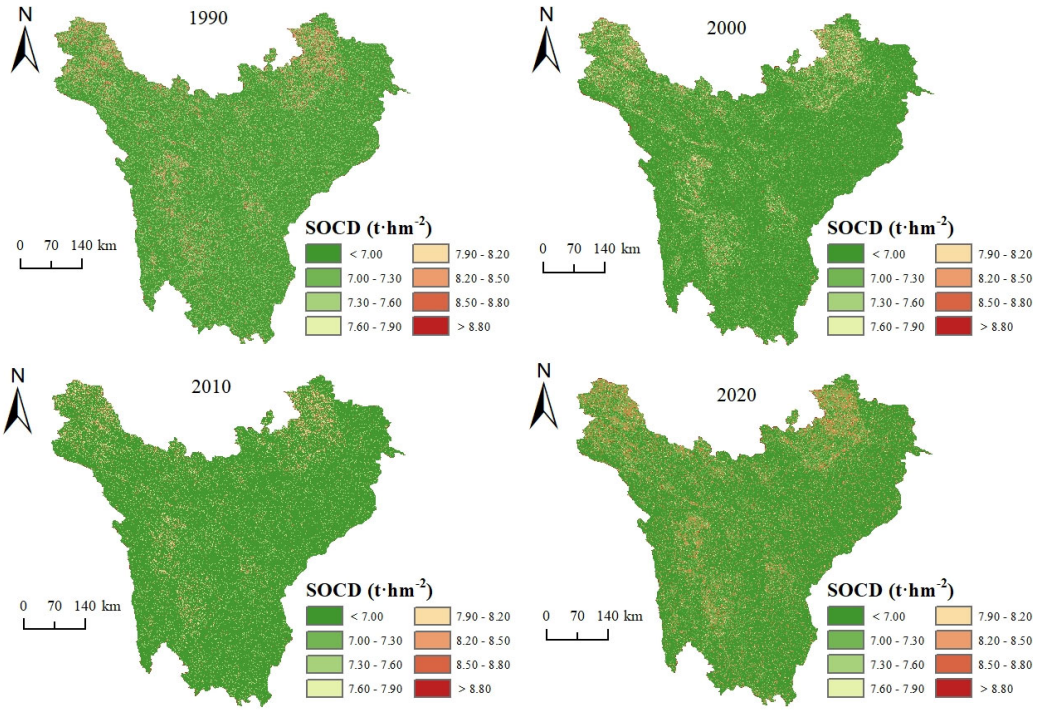

Figure 9. Spatial distribution of SOCD from 1990 to 2020.

3.5. Effects of LUC on SOCS during 1990–2020

We analyzed the spatial distribution of the LUC in the study area from 1990 to 2020 (Figure 10). Considering that forests and grassland were the main sources of the SOCS in the study area, we examined the carbon dynamics and LUC associated with the conversions between forest and grassland (Figure 11). By comparing the changes in the SOCS in the different land use types, we aimed to better understand the implications of LUC on soil carbon dynamics. The land use types were predominantly grassland and forest in the WSP. The changes in the built-up land and barren land were concentrated in the northeastern and western parts of the study area, respectively. Different land management patterns can significantly affect the SOC content of the soil at different depths.

 doi:10.20944/preprints202402.1659.v1

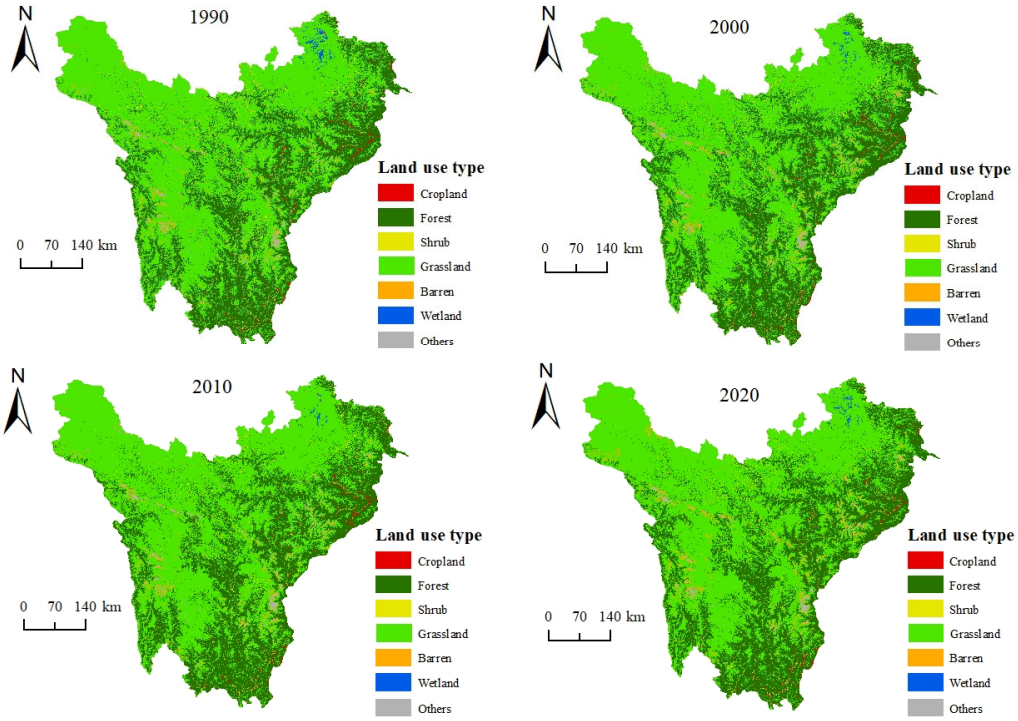

Figure 10. Spatial distribution of land use types in the study area from 1990 to 2020.

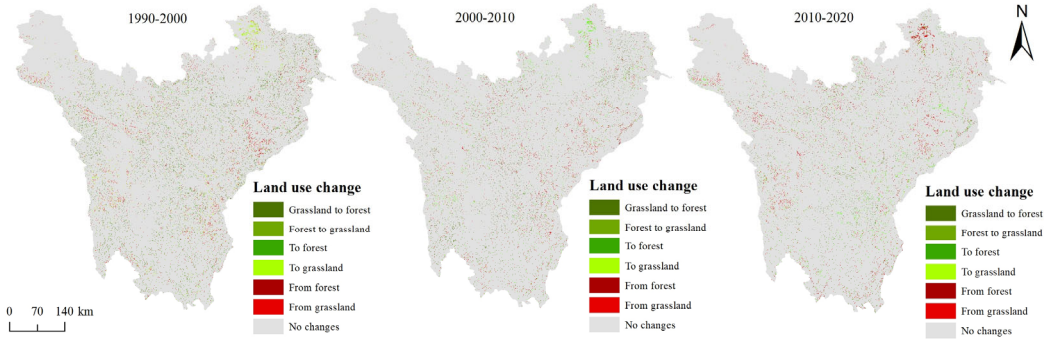

Figure 11. LUC in the study area from 1990 to 2020.

We analyzed the time-series changes of the SOCS from 1990 to 2020 (Table 4) based on the land use changes. The forest and grassland were the main sources of the SOCS. The total SOCS exhibited a decreasing trend during 1990–2010, and the total SOCS increased from 2010 to 2020. The total SOCS increased by 18.03 Tg C from 1990 to 2020, and by 27.88 Tg C from 2010 to 2020. The grassland was the largest region that contributed to the SOCS in the study area during 1990–2020. The SOCS of the cropland was influenced by agricultural management practices and exhibited a decreasing trend. The SOCS of the built-up land with vegetation region was affected by anthropogenic factors and exhibited a clear increasing trend. Land use change affects the activity and diversity of soil microorganisms and influences the stability and cycling processes of SOC. SOC in cropland is the most affected by human activities, as shown by the fact that fertilization patterns during farming could accelerate the rate of decomposition of SOC.

 doi:10.20944/preprints202402.1659.v1

Table 4. SOCSs in the 0–30 cm soil layers for the different land use types.

Land use type	SOCS (Tg C)			
	1990	2000	2010	2020
Cropland	0.91	1.32	1.21	1.18
Forest	72.94	69.92	71.82	88.41
Shrub	2.74	2.33	2.25	2.20
Grassland	135.12	133.57	127.06	137.32
Barren	2.69	2.85	2.54	3.34
Wetland	0.50	0.39	0.17	0.47
Others	0.0041	0.0061	0.0097	0.0186
All	214.9041	210.3861	205.0597	232.9386

4. Discussion

4.1. Impact of Land Management Practices on SOCS

Recently, land use patterns in the study area have undergo significant changes, such as rapid urbanization [48] and land degradation [49]. These changes have had a notable impact on the SOCS in different land use types. Forest and grassland have played a role in enhancing carbon accumulation (Figure 11, Table 4). This finding is consistent with previous studies that have shown the positive effects of grassland and forest sites on SOC. The total SOCS in the study area has improved significantly since 2010 due to the conversion of grassland to forest and wetland. This conclusion is also supported by the results of previous researches [50–52]. In this study, we confirmed that land use transitions can increase the SOCS in the WSP. SOCS in the study area has improved significantly since 2010, with an increase of 27.88 Tg C in the total SOCS compared to 2010. Therefore, to safeguard the stability and sustainability of the SOCS in the study area, it becomes imperative for policymakers to adapt current management practices and policies to preserve and restore degraded ecosystems. Additionally, policymakers should take into account the benefits of forests and grasslands for carbon sequestration.

Moreover, the response of the SOCS to LUC varies with soil depth [53,54]. The SOCD in built-up land exhibited the most pronounced reduction as soil depth increased due to the intense impact of human activities. These activities frequently resulted in soil quality degradation and increased loss of SOC. In contrast, shrub, barren land, grassland, and forest exhibited a higher soil quality due to the high vegetation cover and better sequestration conditions. The wetlands showed the highest stable SOCD trend due to the higher inputs and fixation of SOC. Additionally, this study analyzed the variations in the SOCS among different land use types and soil depths. The findings of this study provided data and theoretical support for enhancing the SOCS in the WSP. Further analyses will be conducted to investigate the effects of factors such as fertilizer and irrigation on the temporal and spatial distribution of the SOCS in different soil depths.

4.2. Uncertainties and Limitations

The results of this study were affected by the variance in the historical image data, primarily due to the inconsistency in the acquisition times of the images for the different years. This can have an impact on the vegetation indices, such as the NDVI, and EVI, and consequently on the SOCS prediction results. Moreover, the temporal-spatial distribution of the SOCS in the study area was synergistically affected by several factors. In this study, we only explored the effects of land use change on the SOCS from qualitative and quantitative perspectives. Further research is still needed to address the synergistic effects of climate change and LUC on the SOCS in the study area. The results of this study showed that there was little data for the regions with higher elevations (Figure 1). In addition, the SOC and SBD data were obtained without considering the specific areas where the land use types have changed. Therefore, if more representative data can be obtained, we can more accurately explore the impact of LUC on SOCS. We will further investigate the future climate and

 doi:10.20944/preprints202402.1659.v1

land use under different scenarios to map the distribution and evolution of the SOCS in the study area.

To verify whether the results of the long-term SOCS are reliable, we compared several measured datasets from previous studies and the HWSD in different years with our simulation results (Figure 6). Strong consistency was found between simulated data and measured data. Moreover, Chen et al. [5] confirmed that the average SOCD in the topsoil in the WSP was 2.00 t m^{-2} in 2020. However, our results indicate that it was 1.96 t m^{-2}, which is lower. This was because we considered the effect of the gravel content and multiple land use types on the SOCD.

5. Conclusions

In this study, we explored the temporal-spatial changes in the LUC on the SOCS in the Western Sichuan Plateau with 30 m spatial resolution. SSA-RFR models and multi-source datasets were utilized to estimate the distribution of SOCS from 1990 to 2020. The vertical distribution of the SOCS in the study area decreased with increasing soil depth, and the SOCS increased from southeast to northwest. The wetlands had the highest SOCD. The grassland, as the main land use type in the study area, had the highest total SOCS (137.32 Tg C in 2020). Forest and grassland were the main sources of the SOCS in the study area, had a significant impact on the increase in the total SOCS. More importantly, land use transitions were confirmed to increase the SOCS in the Western Sichuan Plateau under the climate change. The results of this study confirmed that the SOCS in the study area increased significantly since 2010, with an increase of 27.88 Tg C over the total SOCS in 2010. Further, this study highlighted the importance of land management goals and practices in reaching the dual carbon goals early under the background of climate change. Because the change SOCS is also likely to affect by land management practices including fertilization and cultivation practices. It is crucial to understand the role of land management processes and to discern the effects of management practices to complement the SOCS change estimates provided in this study.

Author Contributions: Z.H.Z.: conceptualization, methodology, software, data curation, visualization, writing—original draft preparation. L.X.: writing—reviewing and editing. Z.F.Z.: methodology, writing—reviewing and editing. F.Z.: writing and editing. G.H.: data curation. S.X.W.: supervision and editing. X.S.: writing—reviewing and editing. S.R.W.: writing—reviewing and editing. P.Y.: writing—reviewing and editing. Y.Z.: funding acquisition. All authors have read and agreed to the published version of the manuscript.

Funding: This research was funded by the National Key Research and Development Program of China, grant number 2022YFF0711803, and the open project of State Key Laboratory of Efficient Utilization of Arid and Semi-arid Arable Land in Northern China, the Institute of Agricultural Resources and Regional Planning, Chinese Academy of Agricultural Sciences, grant number No. EUAL-2023-02.

Data Availability Statement: The data that support the findings of this study are available on request from the corresponding author.

Acknowledgments: The authors thank the USGS for providing Landsat data. We would like to extend our sincere gratitude to the academic editor and reviewers for their constructive comments, which greatly helped us improve the quality of this manuscript.

Conflicts of Interest: The authors declare no conflicts of interest. The funders had no role in the design of the study; in the collection, analyses, or interpretation of data; in the writing of the manuscript; or in the decision to publish the results.

References

1. Gaudaré, U., Kuhnert, M., Smith, P., Martin, M., Barbieri, P., Pellerin, S., Nesme, T. Soil organic carbon stocks potentially at risk of decline with organic farming expansion. Nat. Clim. Change, 2023,13, 719–725.
2. Luo, Z., Wang, G., Wang, E. Global subsoil organic carbon turnover times dominantly controlled by soil properties rather than climate. Nat. Commun. 2019, 10, 3688.
3. Hartley, I.P., Hill, T.C., Chadburn, S.E., Hugelius, G. Temperature effects on carbon storage are controlled by soil stabilisation capacities. Nat. Commun. 2021, 12, 6713.
4. Li, J., Li, M., Zhao, L., Sun, X., Gao, M., Sheng, L., Bian, H. Characteristics of soil carbon emissions and bacterial community composition in peatlands at different stages of vegetation succession. Sci. Total Environ. 2022, 839, 156242.
5. Chen, L., Fang, K., Wei, B., Qin, S., Feng, X., Hu, T., Ji, C., Yang, Y. Soil carbon persistence governed by plant input and mineral protection at regional and global scales. Ecol. Lett. 2021, 24, 1018–1028.
6. Reichenbach, M., Fiener, P., Hoyt, A., Trumbore, S., Six, J., Doetterl, S. Soil carbon stocks in stable tropical landforms are dominated by geochemical controls and not by land use. Glob. Change Biol. 2023, 29, 2591–2607.
7. Beillouin, D., Corbeels, M., Demenois, J., Berre, D., Boyer, A., Fallot, A., Feder, F., Cardinael, R. A global meta-analysis of soil organic carbon in the Anthropocene. Nat. Commun. 2023, 14, 3700.
8. Wang, Z., Li, X., Mao, Y., Li, L., Wang, X., Lin, Q. Dynamic simulation of land use change and assessment of carbon storage based on climate change scenarios at the city level: A case study of Bortala, China. Ecol. Indic. 2022, 134, 108499.
9. Li, H., Wu, Y., Liu, S., Xiao, J., Zhao, W., Chen, J., Alexandrov, G., Cao, Y. Decipher soil organic carbon dynamics and driving forces across China using machine learning. Glob. Change Biol. 2022, 28, 3394–3410.
10. Chen, L., Jing, X., Flynn, D.F.B., Shi, Y., Kühn, P., Scholten, T., He, J.-S. Changes of carbon stocks in alpine grassland soils from 2002 to 2011 on the Tibetan Plateau and their climatic causes. Geoderma, 2017, 288, 166–174.
11. Li, X.-Z., Han, B.-S., Yang, F., Hu, C.-Y., Han, G.-Z., Huang, L.-M. Effects of land use change on soil carbon and nitrogen in purple paddy soil. J. Environ. Manage. 2022, 314, 115122.
12. Wang, M., Guo, X., Zhang, S., Xiao, L., Mishra, U., Yang, Y., Zhu, B., Wang, G., Mao, X., Qian, T., Jiang, T., Shi, Z., Luo, Z. Global soil profiles indicate depth-dependent soil carbon losses under a warmer climate. Nat. Commun. 2022, 13, 5514.
13. Wang, Z., Huang, L., Shao, M. Spatial variations and influencing factors of soil organic carbon under different land use types in the alpine region of Qinghai-Tibet Plateau. Catena, 2023, 220, 106706.
14. Chen, F., Feng, P., Harrison, M.T., Wang, B., Liu, K., Zhang, C., Hu, K. Cropland carbon stocks driven by soil characteristics, rainfall and elevation. Sci. Total Environ. 2023, 862, 160602.
15. Han, D., Hu, Z., Wang, X., Wang, T., Chen, A., Weng, Q., Liang, M., Zeng, X., Cao, R., Di, K., Luo, D., Zhang, G., Yang, Y., He, H., Fan, J., Yu, G. Shift in controlling factors of carbon stocks across biomes on the Qinghai-Tibetan Plateau. Environ. Res. Lett. 2022, 17, 074016.
16. Sun, Y., Ma, J., Zhao, W., Qu, Y., Gou, Z., Chen, H., Tian, Y., Wu, F. Digital mapping of soil organic carbon density in China using an ensemble model. Environ. Res. 2023, 231, 116131.
17. Taghizadeh-Mehrjardi, R., Nabiollahi, K., Kerry, R. Digital mapping of soil organic carbon at multiple depths using different data mining techniques in Baneh region, Iran. Geoderma, 2016, 266, 98–110.
18. Zhang, S., Tian, J., Lu, X., Tian, Q. Temporal and spatial dynamics distribution of organic carbon content of surface soil in coastal wetlands of Yancheng, China from 2000 to 2022 based on Landsat images. Catena, 2023, 223, 106961.
19. Terrer, C., Phillips, R.P., Hungate, B.A., Rosende, J., Pett-Ridge, J., Craig, M.E., Van Groenigen, K.J., Keenan, T.F., Sulman, B.N., Stocker, B.D., Reich, P.B., Pellegrini, A.F.A., Pendall, E., Zhang, H., Evans, R.D., Carrillo, Y., Fisher, J.B., Van Sundert, K., Vicca, S., Jackson, R.B. A trade-off between plant and soil carbon storage under elevated CO2. Nature. 2021, 591, 599–603.
20. Wang, Y., Xiao, J., Ma, Y., Ding, J., Chen, X., Ding, Z., Luo, Y. Persistent and enhanced carbon sequestration capacity of alpine grasslands on Earth's Third Pole. Sci. Adv. 2023, 9, eade6875.
21. Soong, J.L., Castanha, C., Hicks Pries, C.E., Ofiti, N., Porras, R.C., Riley, W.J., Schmidt, M.W.I., Torn, M.S. Five years of whole-soil warming led to loss of subsoil carbon stocks and increased CO 2 efflux. Sci. Adv. 2021, 7, eabd1343.
22. Varney, R.M., Chadburn, S.E., Friedlingstein, P., Burke, E.J., Koven, C.D., Hugelius, G., Cox, P.M. A spatial emergent constraint on the sensitivity of soil carbon turnover to global warming. Nat. Commun. 2020, 11, 5544.
23. Zhang, Z., Ding, J., Zhu, C., Wang, Jinjie, Ge, X., Li, X., Han, L., Chen, X., Wang, Jingzhe. Historical and future variation of soil organic carbon in China. Geoderma, 2023, 436, 116557.
24. Zhou, Y., Webster, R., Viscarra Rossel, R.A., Shi, Z., Chen, S. Baseline map of soil organic carbon in Tibet and its uncertainty in the 1980s. Geoderma, 2019, 334, 124–133.

25. He, L., Tang, Y., 2008. Soil development along primary succession sequences on moraines of Hailuogou Glacier, Gongga Mountain, Sichuan, China. Catena, 2008, 72, 259–269.
26. Gao, X., Xiao, Y., Deng, L., Li, Q., Wang, C., Li, B., Deng, O., Zeng, M. Spatial variability of soil total nitrogen, phosphorus and potassium in Renshou County of Sichuan Basin, China. J. Integr. Agric. 2019, 18, 279–289.
27. Liu, Q.Y., Van Der Hilst, R.D., Li, Y., Yao, H.J., Chen, J.H., Guo, B., Qi, S.H., Wang, J., Huang, H., Li, S.C. Eastward expansion of the Tibetan Plateau by crustal flow and strain partitioning across faults. Nat. Geosci. 2014, 7, 361–365.
28. Azene, B., Zhu, R., Pan, K., Sun, X., Nigussie, Y., Gruba, P., Raza, A., Guadie, A., Wu, X., Zhang, L. Land use change alters phosphatase enzyme activity and phosphatase-harboring microbial abundance in the subalpine ecosystem of southeastern Qinghai-Tibet Plateau, China. Ecol. Indic. 2023, 153, 110416.
29. Ma, Z., Chen, Y., Xu, W., Liu, M. Effects of warming on the stoichiometry of soil microbial biomass and extracellular enzymes in an alpine shrubland. Geoderma, 2023, 430, 116329.
30. Wu, A., You, C., Yin, R., Xu, Z., Zhang, L., Liu, Y., Li, H., Wang, L., Xu, L., Xu, H., Hou, G., Liu, S., Tan, B. Forest Gaps Slow the Humification Process of Fir (Abies faxoniana Rehder & E.H.Wilson) Twig Litter during Eight Years of Decomposition in an Alpine Forest. Forests, 2023, 14, 868.
31. Li, Z., Yang, W., Yue, K., Justine, M.F., He, R., Yang, K., Zhuang, L., Wu, F., Tan, B., Zhang, L., Xu, Z. Effects of snow absence on winter soil nitrogen dynamics in a subalpine spruce forest of southwestern China. Geoderma, 2017, 307, 107–113.
32. Ahirwal, J., Nath, A., Brahma, B., Deb, S., Sahoo, U.K., Nath, A.J. Patterns and driving factors of biomass carbon and soil organic carbon stock in the Indian Himalayan region. Sci. Total Environ. 2021, 770, 145292.
33. Balasubramanian, D., Zhou, W.-J., Ji, H.-L., Grace, J., Bai, X.-L., Song, Q.-H., Liu, Y.-T., Sha, L.-Q., Fei, X.-H., Zhang, X., Zhao, J.-B., Zhao, J.-F., Tan, Z.-H., Zhang, Y.-P. Environmental and management controls of soil carbon storage in grasslands of southwestern China. J. Environ. Manage. 2020, 254, 109810.
34. Ma, K., Zhang, Y., Tang, S., Liu, J. Spatial distribution of soil organic carbon in the Zoige alpine wetland, northeastern Qinghai–Tibet Plateau. Catena, 2016, 144, 102–108.
35. Cao, J., Pan, H., Chen, Z., Shang, H. Dynamics in Stoichiometric Traits and Carbon, Nitrogen, and Phosphorus Pools across Three Different-Aged Picea asperata Mast. Plantations on the Eastern Tibet Plateau. Forests, 2020, 11, 1346.
36. Ding, J., Chen, L., Ji, C., Hugelius, G., Li, Y., Liu, L., Qin, S., Zhang, B., Yang, G., Li, F., Fang, K., Chen, Y., Peng, Y., Zhao, X., He, H., Smith, P., Fang, J., Yang, Y. Decadal soil carbon accumulation across Tibetan permafrost regions. Nat. Geosci. 2017, 10, 420–424.
37. Luan, J., Cui, L., Xiang, C., Wu, J., Song, H., Ma, Q., Hu, Z. Different grazing removal exclosures effects on soil C stocks among alpine ecosystems in east Qinghai–Tibet Plateau. Ecol. Eng. 2014, 64, 262–268.
38. Pang, X.P., Wang, Q., Zhang, J., Xu, H.P., Zhang, W.N., Wang, J., Guo, Z.G. Responses of soil inorganic and organic carbon stocks of alpine meadows to the disturbance by plateau pikas. Eur. J. Soil Sci. 2020, 71, 706–715.
39. Sanderman, J., Hengl, T., Fiske, G., Solvik, K., Adame, M.F., Benson, L., Bukoski, J.J., Carnell, P., Cifuentes-Jara, M., Donato, D., Duncan, C., Eid, E.M., Ermgassen, P.Z., Lewis, C.J.E., Macreadie, P.I., Glass, L., Gress, S., Jardine, S.L., Jones, T.G., Nsombo, E.N., Rahman, M.M., Sanders, C.J., Spalding, M., Landis, E. A global map of mangrove forest soil carbon at 30 m spatial resolution. Environ. Res. Lett. 2018, 13, 055002.
40. Chinilin, A., Savin, I.Yu. Combining machine learning and environmental covariates for mapping of organic carbon in soils of Russia. Egypt. J. Remote Sens. Space Sci. 2023, 26, 666–675.
41. Xiao, J., Chevallier, F., Gomez, C., Guanter, L., Hicke, J.A., Huete, A.R., Ichii, K., Ni, W., Pang, Y., Rahman, A.F., Sun, G., Yuan, W., Zhang, L., Zhang, X. Remote sensing of the terrestrial carbon cycle: A review of advances over 50 years. Remote Sens. Environ. 2019, 233, 111383.
42. Yang, J., Fan, J., Lan, Z., Mu, X., Wu, Y., Xin, Z., Miping, P., Zhao, G. Improved Surface Soil Organic Carbon Mapping of SoilGrids250m Using Sentinel-2 Spectral Images in the Qinghai–Tibetan Plateau. Remote Sens. 2022, 15, 114.
43. Van Der Westhuizen, S., Heuvelink, G.B.M., Hofmeyr, D.P. Multivariate random forest for digital soil mapping. Geoderma, 2023, 431, 116365.
44. Zhang, Z., Wu, S., Zhuang, Q., Li, X., Zeng, F., Xie, C., Hou, G., Luo, G. Joint estimation of aboveground biomass using “Space-Air-Ground” data in the Qilian Mountains, China. Ecol. Indic. 2022, 138, 108866.
45. Gomes, L.C., Faria, R.M., De Souza, E., Veloso, G.V., Schaefer, C.E.G.R., Filho, E.I.F. Modelling and mapping soil organic carbon stocks in Brazil. Geoderma, 2019, 340, 337–350.
46. Wang, Q., Yue, C., Li, X.Q., Liao, P., Li, X.Y. Enhancing robustness of monthly streamflow forecasting model using embedded-feature selection algorithm based on improved gray wolf optimizer. J. Hydrol. 2023, 617, 128995.
47. Zhou, J., Dai, Y., Huang, S., Armaghani, D.J., Qiu, Y. Proposing several hybrid SSA—machine learning techniques for estimating rock cuttability by conical pick with relieved cutting modes. Acta Geotech. 2023, 18, 1431–1446.

 doi:10.20944/preprints202402.1659.v1

48. Zhao, F.J., Ma, Y., Zhu, Y.G., Tang, Z., McGrath, S.P. Soil Contamination in China: Current Status and Mitigation Strategies. Environ. Sci. Technol. 2015, 49, 750–759.
49. Wang, Q.F., Jin, H.J., Mu, C.C., Wu, X.D., Zhao, L., Wu, Q.B. Non-climate environmental factors matter to Holocene dynamics of soil organic carbon and nitrogen in an alpine permafrost wetland, Qinghai–Tibet Plateau. Adv. Clim. Change Res. 2023, 14, 213–225.
50. Hunziker, M., Arnalds, O., Kuhn, N.J. Evaluating the carbon sequestration potential of volcanic soils in southern Iceland after birch afforestation. Soil, 2019, 5, 223–238.
51. Nadal-Romero, E., Khorchani, M., Gaspar, L., Arnáez, J., Cammeraat, E., Navas, A., Lasanta, T. How do land use and land cover changes after farmland abandonment affect soil properties and soil nutrients in Mediterranean mountain agroecosystems? Catena, 2023, 226, 107062.
52. Wiesmeier, M., Hübner, R., Spörlein, P., Geuß, U., Hangen, E., Reischl, A., Schilling, B., Von Lützow, M., Kögel-Knabner, I. Carbon sequestration potential of soils in southeast Germany derived from stable soil organic carbon saturation. Glob. Change Biol. 2014, 20, 653–665.
53. Balesdent, J., Basile-Doelsch, I., Chadoeuf, J., Cornu, S., Derrien, D., Fekiacova, Z., Hatté, C. Atmosphere–soil carbon transfer as a function of soil depth. Nature, 2018, 559, 599–602.
54. Eze, S., Magilton, M., Magnone, D., Varga, S., Gould, I., Mercer, T.G., Goddard, M.R. Meta-analysis of global soil data identifies robust indicators for short-term changes in soil organic carbon stock following land use change. Sci. Total Environ. 2023, 860, 160484.